The Journal of Chemical Physics

Disorder of excitons and trions in monolayer $MoSe_2$

Cite as: J. Chem. Phys. **157**, 211101 (2022); https://doi.org/10.1063/5.0108001
Submitted: 07 July 2022 • Accepted: 23 August 2022 • Accepted Manuscript Online: 19 September 2022 • Published Online: 01 December 2022

Jue Wang, Christina Manolatou, Yusong Bai, et al.

The Journal of Chemical Physics COMMUNICATION scitation.org/journal/jcp

Disorder of excitons and trions in monolayer $MoSe_2$

Cite as: J. Chem. Phys. 157, 211101 (2022); doi: 10.1063/5.0108001
Submitted: 7 July 2022 • Accepted: 23 August 2022 •
Published Online: 1 December 2022

Jue Wang,[1] Christina Manolatou,[2] Yusong Bai,[1] James Hone,[3] Farhan Rana,[2,a)] and X.-Y. Zhu[1,a)]

AFFILIATIONS

[1] Department of Chemistry, Columbia University, New York, New York 10027, USA
[2] School of Electrical and Computer Engineering, Cornell University, Ithaca, New York 14853, USA
[3] Department of Mechanical Engineering, Columbia University, New York, New York 10027, USA

Note: This paper is part of the JCP Special Topic on 40 Years of Colloidal Nanocrystals in JCP.
[a)]**Authors to whom correspondence should be addressed:** farhan.rana@cornell.edu and xyzhu@columbia.edu

ABSTRACT

The optical spectra of transition metal dichalcogenide monolayers are dominated by excitons and trions. Here, we establish the dependence of these optical transitions on the disorder from hyperspectral imaging of h-BN encapsulated monolayer $MoSe_2$. While both exciton and trion energies vary spatially, these two quantities are almost perfectly correlated, with spatial variation in the trion binding energy of only ~0.18 meV. In contrast, variation in the energy splitting between the two lowest energy exciton states is one order of magnitude larger at ~1.7 meV. Statistical analysis and theoretical modeling reveal that disorder results from dielectric and bandgap fluctuations, not electrostatic fluctuations. Our results shed light on disorder in high quality TMDC monolayers, its impact on optical transitions, and the many-body nature of excitons and trions.

Transition metal dichalcogenide (TMDC) monolayers have emerged as the most versatile models for the exploration of many-body semiconductor physics in two-dimensions (2D). The interplay of 2D character and poorly screened Coulomb potential leads to strong many-body effects that dominate the optical properties of TMDCs. Strongly bound excitons, with binding energies in the hundreds of meV, and strongly bound trions, with binding energies in the tens of meV, have been observed in TMDCs.[1–4] These tightly bound excitonic complexes are attractive models for the understanding of many-body interactions in 2D and for opto-electronic applications. However, most 2D materials are strongly affected by disorder[5,6] whose sources include material defects,[7] electrostatic potential fluctuations from variations in local charge distributions,[8,9] dielectric constant variations,[10] and strain-induced bandgap changes.[11,12] Interestingly, as we discuss in this Communication, even state-of-the-art TMDC monolayers with hexagonal boron nitride (h-BN) encapsulation are not immune to disorder. The response of many-body exciton and trion states to disorder can provide valuable insights into both the nature of the disorder and the nature of the excitonic complexes. Here, we carry out hyperspectral imaging of excitons and trions in h-BN encapsulated monolayer $MoSe_2$. We find that both exciton and trion energies are sensitive to variations in the local environment, but these two energies are almost perfectly correlated, in contrast to the behavior of the energy gap between the two lowest exciton states. Statistical analysis of the spatial energy variations, combined with theoretical modeling of exciton and trion states in the presence of disorder, reveals that the sources of the disorder are dielectric constant and electronic bandgap variations of $\Delta\varepsilon \sim 0.08$ and $\Delta E_g \sim 2$–3 meV, respectively.

In experiments, we use the highest quality monolayers exfoliated from flux grown $MoSe_2$ single crystals with low defect density ($\sim 10^{11}$ cm^{-2}), as quantified by scanning tunneling microscope (STM) imaging detailed recently,[13] and large areas (>160 μm^2). Each $MoSe_2$ monolayer is encapsulated in h-BN. The steady-state photoluminescence (PL) spectra [Fig. 1(a)] show two narrow peaks assigned to the lowest energy 1s exciton and the lowest energy trion,[3,4] with mean energies $E_{1s}^{ex} = 1.6465 \pm 0.0001$ eV and $E^{tr} = 1.6214 \pm 0.0001$ eV, respectively. The difference $E_{1s}^{ex} - E^{tr}$ is often referred to as the trion binding energy E_b^{tr}. We use $MoSe_2$ monolayers exfoliated from the highest quality single crystal, with quantified defect density of $8 \pm 5 \times 10^{10}$ cm^{-2} from scanning

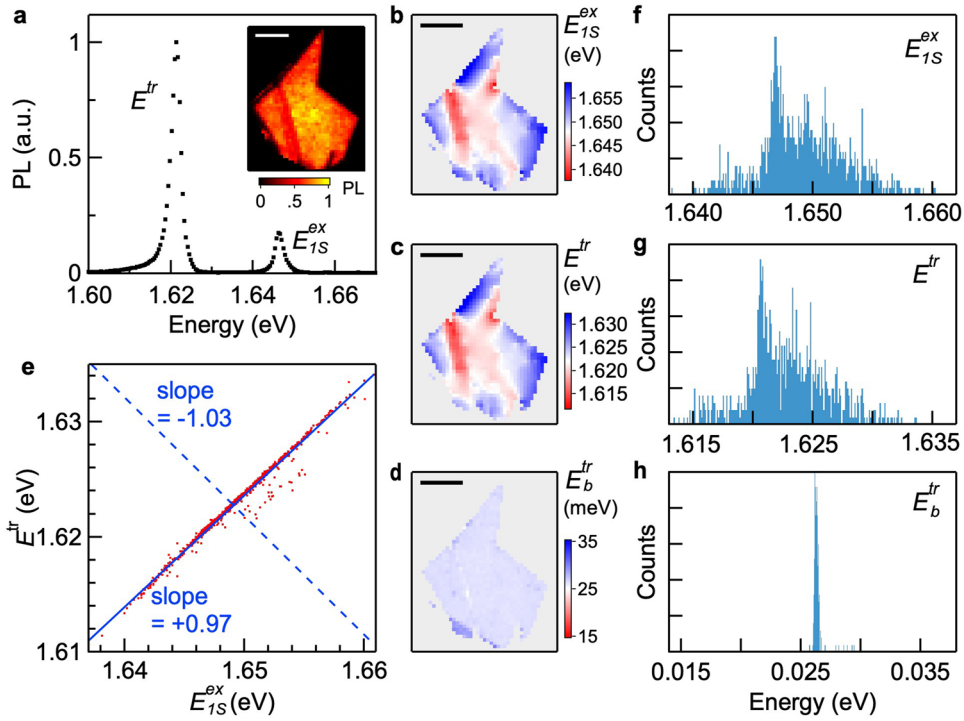

FIG. 1. Insensitivity of the trion binding energy to disorder in monolayer $MoSe_2$. (a) Representative PL spectrum of monolayer $MoSe_2$ encapsulated in h-BN. Inset: total PL intensity image. Scale bar: 5 μm (b)–(d), Spatially resolved exciton peak energy E^{ex}_{1s} (b), trion peak energy E^{tr} (c), and trion binding energy $E^{tr}_b = E^{ex}_{1s} - E^{tr}$ (d) extracted from the PL map. The ranges of color scales are 20 meV. Scale bar: 5 μm. (e) Correlation between trion and exciton peak energies with data points (red dots) extracted from PL mapping. The solid and dashed blue lines indicate the directions of the eigenvectors of the covariance matrix and have slopes of +0.97 and −1.03, respectively. (f)–(h) Histograms of E^{ex}_{1s} (f), E^{tr} (g) and E^{tr}_b (h). The standard deviations in the data are $\sigma^{ex}_{1s} = 3.6 \pm 0.2$ meV (f), $\sigma^{tr} = 3.5 \pm 0.2$ meV (g) and $\sigma^{tr}_b = 0.186 \pm 0.001$ meV (h), respectively. All data shown are taken at a temperature of 4 K.

tunneling microscopy (STM), with calibrated PL quantum yield of 70%, and with full-width-at-half-maximum (FWHM) of both exciton and trion PL peaks approaching ~1 meV, as detailed recently,[13] in agreement with previous reports.[7,14] We determine the effects of disorder[7–12,15–18] by hyperspectral PL imaging with a spatial resolution of ~1 μm. A continuous wave laser at hν = 2.33 eV excites the sample in a diffraction-limited spot of FWHM ~ 0.43 μm, at 4.66 $\mu W/\mu m^2$, corresponding to a calibrated total exciton and trion density of ~1 × $10^{10}/cm^2$.[13] The high sample quality gives rise to relatively homogeneous spatial distributions in total PL intensity [Fig. 1(a), inset] and the trion-to-exciton intensity ratio I_{tr}/I_{ex} [Fig. S1(a)]. Note that we find no correlation between I_{tr} and I_{ex} [Fig. S1(b)], suggesting the absence of measurable electron density fluctuation,[8] which would give rise to anti-correlation in I_{tr} and I_{ex}.

We now focus on E^{ex}_{1s} and E^{tr}, extracted for each spot from intensity-weighted averaging of the PL spectra [Fig. 1(a)]. While E^{ex}_{1s} and E^{tr} fluctuate over the whole sample area [Figs. 1(b) and 1(c)]. The difference between the two shows a surprisingly uniform spatial distribution with a mean value of $E^{tr}_b = 26.220(1) \pm 0.0005$ meV [Fig. 1(d)]. This suggests that spatial fluctuations in E^{ex}_{1s} and E^{tr} are highly correlated. Figure 1(e) shows a scatter plot of E^{tr} vs E^{ex}_{1s}. The solid and dashed lines indicate the directions of the eigenvectors of the covariance matrix of E^{ex}_{1s} and E^{tr} with slopes of +0.97 and −1.03, respectively. Note that slopes of ±1 would indicate perfect correlation and slopes of 0 and ∞ would indicate no correlation. we plot histograms of E^{ex}_{1s}, E^{tr}, and E^{tr}_b in Figs. 1(f)–1(h), corresponding to standard deviations of $\sigma^{ex}_{1s} = 3.6 \pm 0.2$ meV, $\sigma^{tr} = 3.5 \pm 0.2$ meV, and $\sigma^{tr}_b = 0.186 \pm 0.001$ meV, respectively. Because of the nearly perfect correlation between E^{ex}_{1s} and E^{tr}, σ^{tr}_b is only ~5% of σ^{ex}_{1s} and σ^{tr}. The insensitivity of E^{tr}_b to disorder is seen in a broad temperature range until T ~ 60 K, above which the trion PL peak disappears, likely attributed to dissociation of the many-body trion complex by phonon scattering (Figs. S2 and S3).

In stark contrast to the nearly constant E^{tr}_b, the energy splitting between the exciton levels is more broadly distributed. We quantify the spatial distributions in 1*s* and 2*s* exciton energies from reflectance contrast (R_c) spectra on the same sample as in Fig. 1. Figure 2(a) is a representative R_c spectrum showing the A-exciton 1*s* (1.649 eV) and 2*s* (1.799 eV, inset) transitions, and the B-exciton 1*s* transition (1.847 eV), with energies in agreement with previous reports.[10,19] The E^{ex}_{1s} and E^{ex}_{2s} energy maps for the A-1*s* exciton in Figs. 2(b) and 2(c) show characteristic spatial variations attributed to the disorder. The energy gap, $E^{ex}_{\Delta} = E^{ex}_{2s} - E^{ex}_{1s}$, also shows spatial variation of the same order [Fig. 2(d)]. A scatter plot of E^{ex}_{2s} vs E^{ex}_{1s} is shown in Fig. 2(e), along with solid and dashed blue lines showing the directions of the eigenvectors of their covariance matrix. The slopes, +1.44 and −0.69, indicate a much weaker correlation than that between E^{ex}_{1s} and E^{tr}. Figures 2(f)–2(h) show histograms of E^{ex}_{1s} and E^{ex}_{2s}, and E^{ex}_{Δ} with standard deviations $\sigma^{ex}_{1s} = 3.1 \pm 0.2$ meV, $\sigma^{ex}_{2s} = 4.4 \pm 0.4$ meV, and $\sigma^{ex}_{\Delta} = 1.7 \pm 0.1$ meV, respectively. The weak correlation between E^{ex}_{1s} and E^{ex}_{2s} results in σ^{ex}_{Δ} being 40%–60% of σ^{ex}_{2s} and σ^{ex}_{1s}. Note that a comparison of Fig. 2(f) from reflectance and Fig. 1(f) from PL gives a small Stokes shift of −1.5 ± 01 meV, consistent with the low defect density of our sample. Note also that the spin–orbit splitting in the valence band, as reflected in the difference between A and B exciton energies, is an intrinsic property of the monolayer and is robust against spatial variations, Fig. S4.

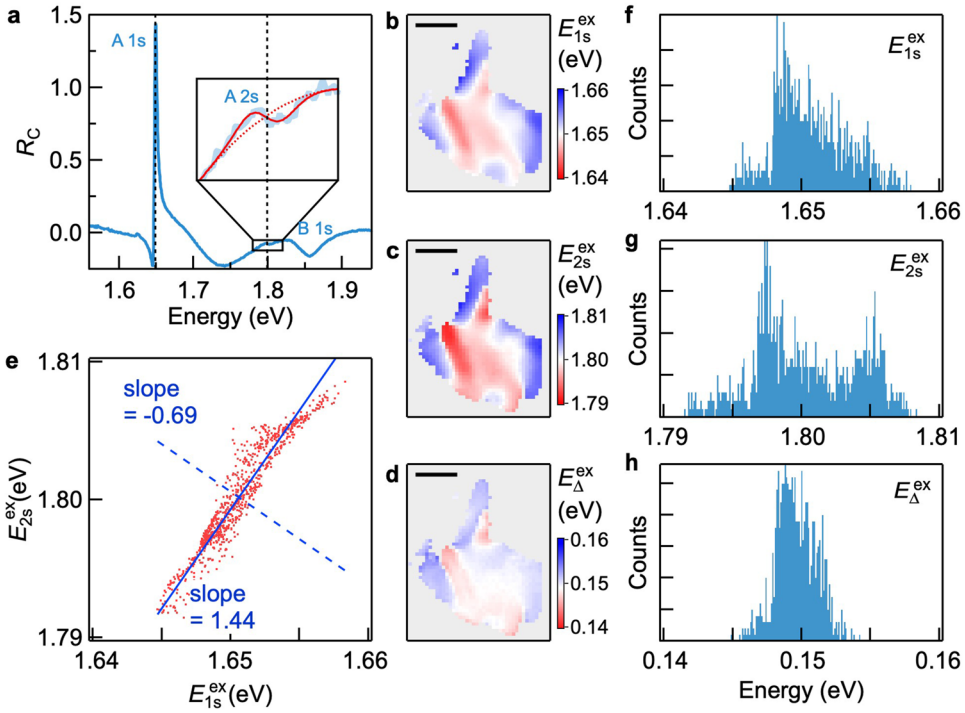

FIG. 2. Spatial fluctuation of the exciton energy level splitting in monolayer MoSe2. (a) A 1s (1.649 eV), A 2s (1.799 eV) and B 1s resonances. Inset: Fit (red line) to R_C around the A 2s resonance (light blue line). (b)–(d) Spatially resolved exciton peak energies E_{1s}^{ex} (b), E_{2s}^{ex} (c) and $E_{\Delta}^{ex} = E_{2s}^{ex} - E_{1s}^{ex}$, (d) extracted from R_C spectral image. All three color scales span 20 meV. Scale bar: 5 μm. (e) Correlation between E_{2s}^{ex} and E_{1s}^{ex} exciton energies (red dots). The solid and dashed blue lines indicate the directions of the eigenvectors of the covariance matrix with slopes of +1.44 and −0.69, respectively. (f)–(h) Histograms of the exciton energies E_{1s}^{ex} (f), E_{2s}^{ex} (g) and the energy difference E_{Δ}^{ex} (h). The respective standard deviations are 3.08 ± 0.05, 4.37 ± 0.05 and 1.73 ± 0.05 meV. The mean value of 2s-1s energy difference E_{Δ}^{ex} is 149.46 ± 0.05 meV. All data shown are taken at a temperature of 4 K.

The covariance matrices $K^a(E_{1s}^{ex}, E_{2s}^{ex})$ and $K^b(E_{1s}^{ex}, E^{tr})$ can be used to understand the nature of the disorder. These matrices are obtained from the data (in units of meV^2),

$$K^a(E_{1s}^{ex}, E_{2s}^{ex}) = \begin{bmatrix} 9.4763 & 12.7781 \\ 12.7781 & 19.0697 \end{bmatrix},$$
$$K^b(E_{1s}^{ex}, E^{tr}) = \begin{bmatrix} 12.8235 & 12.4329 \\ 12.4329 & 12.0843 \end{bmatrix}. \quad (1)$$

The determinants of both covariance matrices are non-zero, *implying that more than one disorder mechanism is responsible for the observed spatial variations in the exciton and trion energies.* We consider the effects of two different types of spatial disorder on E_{Δ}^{ex} and E_b^{tr}: (i) electronic bandgap variations due to strain[11,12] and (ii) disorder in the dielectric constant of the media surrounding the 2D monolayer.[10] In the supplementary material, we discuss potential disorder and explain why it is inconsistent with our experimental observations.

Recent many body models have shown that the PL peaks observed in the measured optical spectra correspond to a superposition of exciton and trion states,[20] (also called exciton-polaron states[21–23]), rather than to pure exciton or pure trion states. Furthermore, the trions states involved in this superposition are four-body neutral states[20] and not three-body charged states, as is commonly assumed. However, given the small electron density in our samples ($\leq 10^{11}$ cm^{-2}) as quantitatively determined by exciton/trion intensities and STM imaging,[13] one can safely assume, in light of the model of Rana *et al.*,[20] that the observed lowest energy exciton-trion superposition state in our PL spectrum is essentially a four-body bound trion state (E_{1s1s}^{tr}) and the higher energy superposition states in PL and R_c spectra are essentially two-body bound exciton states (E_{1s}^{ex} and E_{2s}^{ex}). If $\vec{R}$ is the center of mass coordinate of the exciton (or trion), the local shifts in the exciton and trion energies can be written as

$$\Delta E_{ns}^{ex}(\vec{R}) = \Delta E_g^{S,T}(\vec{R}) + (\gamma_g + \gamma_{b-ns}^{ex})\Delta\varepsilon_{ext}(\vec{R}),$$
$$\Delta E^{tr}(\vec{R}) = \Delta E_g^{S,T}(\vec{R}) + (\gamma_g + \gamma_{b-1s}^{ex} + \gamma_b^{tr})\Delta\varepsilon_{ext}(\vec{R}). \quad (2)$$

Here, $\Delta E_g^{S,T}$ is the variation in the bandgap attributed to strain, the coefficient $\gamma_g = \partial E_g/\partial\varepsilon_{ext}$ describes the change in the bandgap due to dielectric disorder, the coefficients $\gamma_{b-ns}^{ex} = -\partial E_{b-ns}^{ex}/\partial\varepsilon_{ext}$ and $\gamma_b^{tr} = -\partial E_b^{tr}/\partial\varepsilon_{ext}$ describe the changes in the exciton and trion *binding* energies, respectively, due to dielectric disorder, and $\Delta\varepsilon_{ext}(\vec{R})$ represents the variation in the (relative) dielectric constant of the media surrounding the monolayer.[10] Note that ε_{ext} is the average of the dielectric constants of the media on the top and bottom sides of the monolayer. The value of γ_g can be obtained as the change in the energy of a hole due to dielectric polarization charges [Fig. 3(a)] in a thin film of thickness d, of bulk dielectric constant ε_{bulk}, and surrounded by a medium of dielectric constant ε_{ext}, when ε_{ext} changes by a small amount,[20]

$$\gamma_g = \frac{\partial}{\partial\varepsilon_{ext}} \int \frac{d^2\vec{q}}{(2\pi)^2} \frac{e}{2\varepsilon_o q}\left[\frac{1}{\varepsilon_{2D}(q)} - \frac{1}{\varepsilon_{bulk}}\right], \quad (3)$$

where the dielectric constant $\varepsilon_{2D}(q)$ is given by[20]

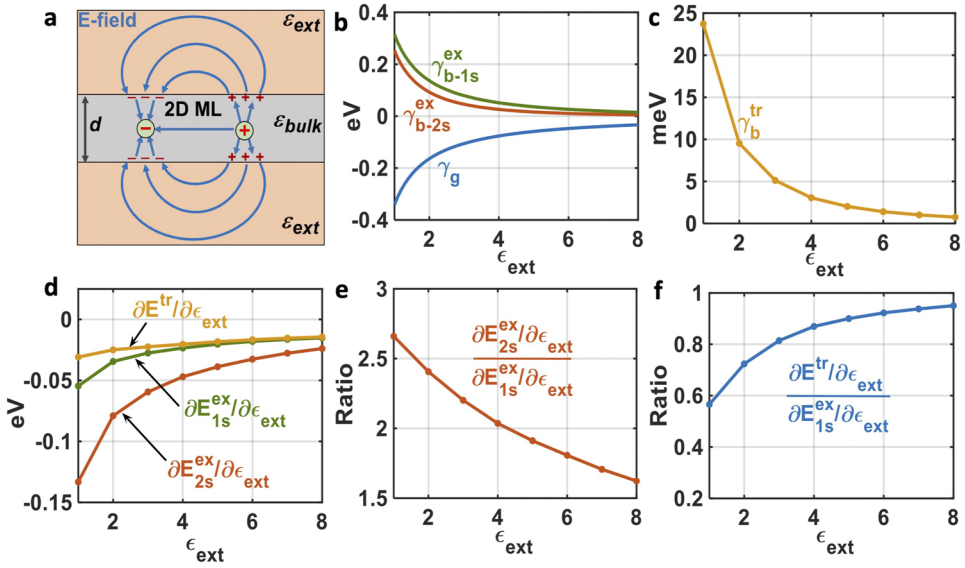

FIG. 3. Theoretical model. (a) Dielectric polarization charge, which renormalizes the bandgap of a TMD monolayer, is depicted for the case $\varepsilon_{bulk} > \varepsilon_{ext}$. (b) and (c) The coefficients $\gamma_g = \partial E_g/\partial\varepsilon_{ext}$, $\gamma^{ex}_{b-1s} = -\partial E^{ex}_{b-1s}/\partial\varepsilon_{ext}$, and $\gamma^{ex}_{b-2s} = -\partial E^{ex}_{b-2s}/\partial\varepsilon_{ext}$ (b) and $\gamma^{tr}_b = -\partial E^{ex}_b/\partial\varepsilon_{ext}$ (c) that describe bandgap renormalization, and the sensitivities of the binding energies of the 2*s* and the 1*s* exciton levels and the trion level, respectively, are plotted as functions of ε_{ext}. (d) The sensitivities of the energies of the 2*s* and the 1*s* exciton levels and the trion level, including bandgap renormalization, are plotted as a function of ε_{ext}. (e) and (f), The relative sensitivities of the energies of the 2*s* and 1*s* exciton levels (e), and of the trion and 1*s* exciton levels (f), with respect to changes in ε_{ext}.

$$\varepsilon(q) = \varepsilon_{bulk}\frac{(1+\varepsilon_{bulk}/\varepsilon_{ext}) + (1-\varepsilon_{bulk}/\varepsilon_{ext})e^{-qd}}{(1+\varepsilon_{bulk}/\varepsilon_{ext}) - (1-\varepsilon_{bulk}/\varepsilon_{ext})e^{-qd}}. \tag{4}$$

The values of γ^{ex}_{b-ns} and γ^{tr}_b can be computed using methods discussed previously.[20] The results are shown in Figs. 3(b) and 3(c). Consistent with a previous report,[10] our calculations show that effects due to bandgap renormalization and exciton binding energy shift almost cancel each other for the 1*s* exciton state such that $|\partial E^{ex}_{2s}/\partial\varepsilon_{ext}|$ for the 2*s* exciton state is almost exactly a factor of two larger than $|\partial E^{ex}_{1s}/\partial\varepsilon_{ext}|$ when $\varepsilon_{ext} \sim 4$ (the dielectric constant of h-BN) [Figs. 3(d) and 3(e)]. We also find that the trion energy closely tracks the 1*s* exciton energy such that $|\partial E^{tr}/\partial\varepsilon_{ext}|$ is ~0.87$|\partial E^{ex}_{1s}/\partial\varepsilon_{ext}|$ when $\varepsilon_{ext} \sim 4$ [Figs. 3(d) and 3(f)]. Assuming that $\Delta E^{S,T}_g(\vec{R})$ and $\Delta\varepsilon_{ext}(\vec{R})$ are statistically independent, the following quantities can be obtained directly from the covariance matrices of our data given in Eq. (1),

$$\frac{\partial E^{ex}_{2s}/\partial\varepsilon_{ext}}{\partial E^{ex}_{1s}/\partial\varepsilon_{ext}} = \frac{K^a_{12}(E^{ex}_{1s},E^{ex}_{2s}) - K^a_{22}(E^{ex}_{1s},E^{ex}_{2s})}{K^a_{11}(E^{ex}_{1s},E^{ex}_{2s}) - K^a_{12}(E^{ex}_{1s},E^{ex}_{2s})} = 1.91, \tag{5}$$

$$\frac{\partial E^{tr}/\partial\varepsilon_{ext}}{\partial E^{ex}_{1s}/\partial\varepsilon_{ext}} = \frac{K^b_{12}(E^{ex}_{1s},E^{tr}) - K^b_{22}(E^{ex}_{1s},E^{tr})}{K^b_{11}(E^{ex}_{1s},E^{tr}) - K^b_{12}(E^{ex}_{1s},E^{tr})} = 0.89. \tag{6}$$

The experimentally determined values of 1.91 and 0.89 for the ratios above are in remarkably agreement with the respective theoretical values of 2.03 and 0.87 (for $\varepsilon_{ext} \sim 4$). This agreement shows that the model given in Eq. (2) captures the essential physics. In the supplementary material, we show that $\partial E^{ex}_{2s}/\partial E^{ex}_{1s}$ calculated in the case of potential disorder is given by the ratio of the polarizabilities of the 2*s* and 1*s* exciton states and equals ~102, which is ~53 times larger than the measured value of 1.91. We, therefore, conclude that potential disorder is not the main contributor to the variations in exciton and trion energies in our samples.

Based on Eq. (2), one can also use the covariance matrices to obtain root mean square values $\sqrt{\langle(\Delta E^{S,T}_g)^2\rangle}$ and $\sqrt{\langle(\Delta\varepsilon_{ext})^2\rangle}$ from the following relations:

$$\sqrt{\langle(\Delta\varepsilon_{ext})^2\rangle} = \frac{1}{|\partial E^{ex}_{1s}/\partial\varepsilon_{ext}|}\sqrt{\frac{\left(K^{a/b}_{11}-K^{a/b}_{12}\right)^2}{K^{a/b}_{11}+K^{a/b}_{22}-2K^{a/b}_{12}}},$$
$$\sqrt{\langle(\Delta E^{S,T}_g)^2\rangle} = \sqrt{\frac{K^{a/b}_{11}K^{a/b}_{22}-\left(K^{a/b}_{12}\right)^2}{K^{a/b}_{11}+K^{a/b}_{22}-2K^{a/b}_{12}}}. \tag{7}$$

Using the theoretical value ~23.5 meV of $|\partial E^{ex}_{1s}/\partial\varepsilon_{ext}|$ [Fig. 3(d)], we find that $\sqrt{\langle(\Delta\varepsilon_{ext})^2\rangle}$ equals 0.0813 if we use the covariance matrix $K^a(E^{ex}_{1s},E^{ex}_{2s})$ and 0.0810 if we use the covariance matrix $K^b(E^{ex}_{1s},E^{tr})$. This remarkable agreement between the values of $\sqrt{\langle(\Delta\varepsilon_{ext})^2\rangle}$ obtained using two different experimental techniques (PL and reflection spectroscopies) that looked at two different energy level differences (between 2*s* and 1*s* exciton levels in the case of reflection spectroscopy and between 1*s* exciton and trion levels in the case of PL) further supports the validity of our theoretical model. The values of $\sqrt{\langle(\Delta E^{S,T}_g)^2\rangle}$ come out to be 2.4 and 2.9 meV if we use the covariance matrices $K^a(E^{ex}_{1s},E^{ex}_{2s})$ and $K^b(E^{ex}_{1s},E^{tr})$, respectively. These $\sqrt{\langle(\Delta\varepsilon_{ext})^2\rangle}$ values are in satisfactory agreement given the very different experimental measurements.

We point out that the use of the state-of-the-art sample of the lowest defect density to date[13] is key to the first quantitative comparison between experiment and theory on exciton and trion disorder in a TMDC monolayer. This comparison identifies

excitonic disorder as resulting from dielectric fluctuation and strain-related bandgap changes, not electrostatic variation. While dielectric fluctuation may come from impurity charges and adsorbates,[10] strain may have intrinsic origin due to atomic scale relaxation at interface,[24] and extrinsic sources from the transfer stacking process[25] or roughness of the substrate.[5] Further minimizing disorder may necessitate the development of automated transfer stacking processes in ultra-clean environments. We note that previous spectroscopic efforts in exploring the disorder problem have focused on distinguishing homogeneous from heterogeneous linewidth of exciton transitions from coherent spectroscopies.[26–28] In a four-wave mixing experiment on exciton-trion coherence, Jakubczyk *et al.* also reported a nearly constant trion binding energy despite the presence of more extensive spatial disorder from the use of more defective samples without encapsulation; these authors noted the interesting observation without providing an interpretation.[28]

In conclusion, we have compared the behaviors of excitons and trions in the presence of disorder in monolayer $MoSe_2$ encapsulated in h-BN. Hyperspectral imaging revealed that the 2*s*-1*s* exciton energy splitting varies by $\sigma_{\Delta}^{ex} = 1.7 \pm 0.1$ meV due to disorder. In contrast, the trion binding energy is robust with spatial variation of only $\sigma_{b}^{tr} = 0.186 \pm 0.001$ meV, which is one order of magnitude lower than σ_{Δ}^{ex}. Theoretical analysis based on the many-body exciton-trion quantum superposition model[20] provides a quantitative explanation of the experimental results and suggests dielectric and strain origins, not an electrostatic one, for exciton and trion disorder.

See the supplementary material for methods, additional data, and analysis (Figures S1–S5).

ACKNOWLEDGMENTS

The experimental work was supported by the Materials Science and Engineering Research Center (MRSEC) through NSF Grant No. DMR-2011738. Sample preparation was supported by the Vannevar Bush Faculty Fellowship program through Office of Naval Research Grant No. N00014-18-1-2080. We thank Kenji Watanabe and Takashi Taniguchi for providing h-BN crystals and Wenjing Wu, Lin Zhou, and Song Liu for help with sample fabrication. The theoretical work was supported by CCMR under NSF-NRSEC Grant No. DMR-1719875, NSF EFRI-NewLaw under Grant No. 1741694, and AFOSR under Grant No. FA9550-19-1-0074.

AUTHOR DECLARATIONS

Conflict of Interest

The authors have no conflicts to disclose.

Author Contributions

Jue Wang: Conceptualization (equal); Data curation (equal); Formal analysis (equal); Investigation (equal); Methodology (equal); Validation (equal); Visualization (equal); Writing – original draft (equal). **Christina Manolatou**: Data curation (equal); Formal analysis (equal); Investigation (equal); Methodology (equal); Software (equal). **Yusong Bai**: Data curation (equal); Methodology (equal). **James Hone**: Methodology (equal). **Farhan Rana**: Conceptualization (equal); Formal analysis (equal); Investigation (equal); Resources (equal); Software (equal); Writing – review & editing (equal). **X.-Y. Zhu**: Conceptualization (equal); Formal analysis (equal); Funding acquisition (lead); Project administration (lead); Supervision (lead); Writing – original draft (lead).

DATA AVAILABILITY

The data that support the findings of this study are available within the article and its supplementary material.

REFERENCES

[1] K. F. Mak, C. Lee, J. Hone, J. Shan, and T. F. Heinz, Phys. Rev. Lett. **105**, 136805 (2010).
[2] A. Splendiani, L. Sun, Y. Zhang, T. Li, J. Kim, C.-Y. Chim, G. Galli, and F. Wang, Nano Lett. **10**, 1271 (2010).
[3] J. S. Ross, S. Wu, H. Yu, N. J. Ghimire, A. M. Jones, G. Aivazian, J. Yan, D. G. Mandrus, D. Xiao, W. Yao, and X. Xu, Nat. Commun. **4**, 1474 (2013).
[4] K. F. Mak, K. He, C. Lee, G. H. Lee, J. Hone, T. F. Heinz, and J. Shan, Nat. Mater. **12**, 207 (2013).
[5] D. Rhodes, S. H. Chae, R. Ribeiro-Palau, and J. Hone, Nat. Mater. **18**, 541 (2019).
[6] S. M. Hus and A.-P. Li, Prog. Surf. Sci. **92**, 176 (2017).
[7] D. Edelberg, D. Rhodes, A. Kerelsky, B. Kim, J. Wang, A. Zangiabadi, C. Kim, A. Abhinandan, J. Ardelean, M. Scully, D. Scullion, L. Embon, R. Zu, E. J. G. Santos, L. Balicas, C. Marianetti, K. Barmak, X. Zhu, J. Hone, and A. N. Pasupathy, Nano Lett. **19**, 4371 (2019).
[8] J. Martin, N. Akerman, G. Ulbricht, T. Lohmann, J. H. Smet, K. Von Klitzing, and A. Yacoby, Nat. Phys. **4**, 144 (2008).
[9] J. Xue, J. Sanchez-Yamagishi, D. Bulmash, P. Jacquod, A. Deshpande, K. Watanabe, T. Taniguchi, P. Jarillo-Herrero, and B. J. Leroy, Nat. Mater. **10**, 282 (2011).
[10] A. Raja, L. Waldecker, J. Zipfel, Y. Cho, S. Brem, J. D. Ziegler, M. Kulig, T. Taniguchi, K. Watanabe, E. Malic, T. F. Heinz, T. C. Berkelbach, and A. Chernikov, Nat. Nanotechnol. **14**, 832 (2019).
[11] B. G. Shin, G. H. Han, S. J. Yun, H. M. Oh, J. J. Bae, Y. J. Song, C.-Y. Park, and Y. H. Lee, Adv. Mater. **28**, 9378 (2016).
[12] H. Peelaers and C. G. Van de Walle, Phys. Rev. B **86**, 241401 (2012).
[13] B. Kim, Y. Luo, D. Rhodes, Y. Bai, J. Wang, S. Liu, A. Jordan, B. Huang, Z. Li, T. Taniguchi, K. Watanabe, J. Owen, S. Strauf, K. Barmak, X. Zhu, and J. Hone, ACS Nano **16**, 140 (2022).
[14] O. A. Ajayi, J. V. Ardelean, G. D. Shepard, J. Wang, A. Antony, T. Taniguchi, K. Watanabe, T. F. Heinz, S. Strauf, X.-Y. Zhu, and J. C. Hone, 2D Mater. **4**, 031011 (2017).
[15] A. Raja, A. Chaves, J. Yu, G. Arefe, H. M. Hill, A. F. Rigosi, T. C. Berkelbach, P. Nagler, C. Schüller, T. Korn, C. Nuckolls, J. Hone, L. E. Brus, T. F. Heinz, D. R. Reichman, and A. Chernikov, Nat. Commun. **8**, 15251 (2017).
[16] Y. Lin, X. Ling, L. Yu, S. Huang, A. L. Hsu, Y.-H. Lee, J. Kong, M. S. Dresselhaus, and T. Palacios, Nano Lett. **14**, 5569 (2014).
[17] E. Courtade, M. Semina, M. Manca, M. M. Glazov, C. Robert, F. Cadiz, G. Wang, T. Taniguchi, K. Watanabe, M. Pierre, W. Escoffier, E. L. Ivchenko, P. Renucci, X. Marie, T. Amand, and B. Urbaszek, Phys. Rev. B **96**, 085302 (2017).
[18] D. Van Tuan, M. Yang, and H. Dery, Phys. Rev. B **98**, 125308 (2018).
[19] B. Han, C. Robert, E. Courtade, M. Manca, S. Shree, T. Amand, P. Renucci, T. Taniguchi, K. Watanabe, X. Marie, L. E. Golub, M. M. Glazov, and B. Urbaszek, Phys. Rev. X **8**, 031073 (2018).
[20] F. Rana, O. Koksal, and C. Manolatou, Phys. Rev. B **102**, 085304 (2020).
[21] D. K. Efimkin and A. H. MacDonald, Phys. Rev. B **95**, 035417 (2017).
[22] D. K. Efimkin, E. K. Laird, J. Levinsen, M. M. Parish, and A. H. MacDonald, Phys. Rev. B **103**, 075417 (2021).

[23]M. Sidler, P. Back, O. Cotlet, A. Srivastava, T. Fink, M. Kroner, E. Demler, and A. Imamoglu, Nat. Phys. **13**, 255 (2017).
[24]S. Shabani, D. Halbertal, W. Wu, M. Chen, S. Liu, J. Hone, W. Yao, D. N. Basov, X. Zhu, and A. N. Pasupathy, Nat. Phys. **17**, 720 (2021).
[25]Y. Bai, L. Zhou, J. Wang, W. Wu, L. J. McGilly, D. Halbertal, C. F. B. Lo, F. Liu, J. Ardelean, P. Rivera, N. R. Finney, X.-C. Yang, D. N. Basov, W. Yao, X. Xu, J. Hone, A. N. Pasupathy, and X.-Y. Zhu, Nat. Mater. **19**, 1068 (2020).
[26]G. Moody, C. Kavir Dass, K. Hao, C.-H. Chen, L.-J. Li, A. Singh, K. Tran, G. Clark, X. Xu, G. Berghäuser, E. Malic, A. Knorr, and X. Li, Nat. Commun. **6**, 8315 (2015).
[27]E. W. Martin, J. Horng, H. G. Ruth, E. Paik, M.-H. Wentzel, H. Deng, and S. T. Cundiff, Phys. Rev. Appl. **14**, 021002 (2020).
[28]T. Jakubczyk, V. Delmonte, M. Koperski, K. Nogajewski, C. Faugeras, W. Langbein, M. Potemski, and J. Kasprzak, Nano Lett. **16**, 5333 (2016).